DOI: 10.1002/chem.200801447

The Structure-Controlling Solventless Synthesis and Optical Properties of Uniform Cu_2S Nanodisks

Yu-Biao Chen, Ling Chen, and Li-Ming Wu*[a]

Abstract: Uniform Cu_2S nanodisks have been synthesized from a well-characterized layered copper thiolate precursor by structure-controlling solventless thermolysis at 200–220 °C under a N_2 atmosphere. The development from small Cu_2S nanoparticles (diameter ≈3 nm) to nanodisks (diameter 8.3 nm) and then to faceted nanodisks (diameter 27.5 nm, thickness 12.7 nm) is accompanied by a continuous phase transition from metastable orthorhombic to monoclinic Cu_2S, the ripening of small particles by aggregation, and finally the crystallization process. The growth of the nanoproduct is constrained by the crystal structure of the precursor and the in situ-generated thiol molecules. Such controlled anisotropic growth leads to a nearly constant thickness of faceted nanodisks with different diameters, which has been confirmed by TEM observations and optical absorption measurements.

Keywords: aggregation · layered compounds · nanostructures · optical properties · solventless method

Introduction

Nanocrystalline semiconductors have been extensively investigated because of their unique physical–chemical properties.[1–3] Generally, these properties are heavily dependent on the size and morphology,[4,5] and nanocrystals with anisotropic features, such as nanowires, nanorods, nanotubes, nanoribbons, nanofilms, nanodisks, nanoplates, nanocubes, and nanoprisms, have more advantages over nanospheres in technological application.[6–9] Among these examples, lamellar nanostructures are a favorite for the fabrication of nanodevices; for example, anisotropic nanodisks are very good building blocks for constructing nanodevices, with the crystal orientation controlled by a bottom-up method.[10–13]

The newly established solventless thermolytic method has proved to be successful in producing anisotropic nanomaterials.[14–20] As a first example, uniform Ag nanodisks were obtained by the thermolysis of layered precursor $AgSC_{12}H_{25}$, which has large interlayer spaces. The disk morphology is proposed to be self-controlled on the atomic level by the structure of the precursor.[18] However, the thickness of the Ag nanodisks (≈2.3 nm) is about 15 times larger than the 1.5 Å thickness of the central Ag/S slab of the precursor, and the reviewers raised a doubt concerning the mechanism of this layered-precursor-to-lamellar-nanoproduct (LPLP) conversion. Unfortunately, an intermediate between the precursor and the nanoproduct is not currently available, but an isostructural Bi precursor, $Bi(SC_{12}H_{25})_3$, has subsequently been synthesized. The interruption of the thermolysis process of this Bi precursor at an early stage during heating allowed the capture of an amorphous Bi nanofilm several atoms in thickness (0.6 nm), which sustains the idea that the early growth is constrained by the layered structure of the Bi precursor. A parallel experiment without interruption generated monolayer arrays of large lamellar nanorhombi (≈22 nm in length and ≈0.9 nm in height).[19] Although the physical layered arrangement of the rhombi and their uniform lamellar morphology suggest some relation to the nanofilm, an intermediate between small nanoparticles and large nanorhombi is still needed and therefore, there is still a great degree of guesswork in the interpretation of the late growth stage of the LPLP conversion. Herein, we present interesting and important observations regarding Cu_2S to illustrate the late growth stage. These facts, together with previous observations on nanofilms[19] and Ag disks,[18] substantiate the whole growth mechanism of a structure-controlling solventless method.

[a] Dr. Y.-B. Chen, Prof. Dr. L. Chen, Prof. L.-M. Wu
State Key Laboratory of Structural Chemistry
Fujian Institute of Research on the Structure of Matter
Chinese Academy of Sciences
Fuzhou 350002 (China)
Fax: (+86) 591-8370-4947
E-mail: Liming_Wu@fjirsm.ac.cn

Supporting information for this article is available on the WWW under http://dx.doi.org/10.1002/chem.200801447.

Bulk Cu_2S (band gap energy $E_g = 1.21$ eV) has been extensively investigated and used as a solar cell material.[21,22] The quantum size effect of nano Cu_2S materials[23] results in the tunable band gaps of these materials, which is desirable in photoelectric applications. Recently, Cu_2S nanocrystals with different morphologies, such as wires,[17,24,25] ribbons,[26,27] tubes,[25] rods,[14] disks, and plates,[10,13,14] have been prepared by using different approaches, for example, solid, solution, hydrothermal, and solventless methods. The solventless method has shown advantages in producing uniform nanoproducts,[14,17] however, high yields from this method are impossible because of the extreme difficulty of separating Cu_2S nanoproducts from the raw products (a mixture of several insoluble byproducts and unreacted reactants). Herein, we utilize $[Cu(SC_{12}H_{25})_2]$ as a precursor, in place of a mixture of copper salt, thiol, and surfactants, to produce uniform Cu_2S nanodisks on a gram scale. The possible formation mechanism and the dependence of optical properties on the morphology and size are also reported.

Results and Discussion

Structure and thermal properties of the $[Cu(SC_{12}H_{25})_2]$ precursor: The yellow-green powdery precursor was synthesized from a 4:1 molar ratio of 1-dodecanethiol and copper nitrate in ethanol and water (see the Experimental Section). The excess dodecanethiol ensured the complete precipitation of Cu^{2+} ions. The formula of the precursor was determined to be $[Cu(SC_{12}H_{25})_2]$ by using elemental analysis, which also satisfies the charge-balance requirement. The powder X-ray diffraction (PXRD) pattern of the $[Cu(SC_{12}H_{25})_2]$ precursor (after the excess dodecanethiol was washed off) is presented in Figure 1. The intense narrow reflections correspond to successive $0k0$ ($k = 2$–9) orders of the diffractions from a layered structure with a large d spacing and preferred orientation. The measured kd values of all 8 reflections fall within the range 35.67 to 35.94 Å, with an average of 35.81 Å (see the Supporting Information, Table S1), which is about twice the expected length of the alkyl chain (L). This layered motif is similar to that of silver and bismuth dodecanethiolate,[18,19] which have interlayer spacings of 34.6 and 31.49 Å, respectively. Therefore, the structure of as-synthesized $[Cu(SC_{12}H_{25})_2]$ is also proposed to consist of a central layer of Cu/S with the alkyl chain tails extending out from both sides of the central layer. The interlayer distance of $[Cu(SC_{12}H_{25})_2]$ (≈ 2 L) is larger than that of the silver or bismuth analogues, which may result from different features of the intralayer structure. We have not successfully obtained a suitable single crystal of $[Cu(SC_{12}H_{25})_2]$, which is needed to determine the detailed intralayer structure not revealed by the powder diffraction patterns. However, knowing the anisotropic layered nature of the $[Cu(SC_{12}H_{25})_2]$ precursor gives some helpful insights into the LPLP conversion process.

The temperature dependence of the decomposition of the $[Cu(SC_{12}H_{25})_2]$ precursor was examined by differential thermal analysis, thermogravimetric analysis, and quadrupole mass spectrometry (DTA/TG/QMS; Figure 2). The DTA

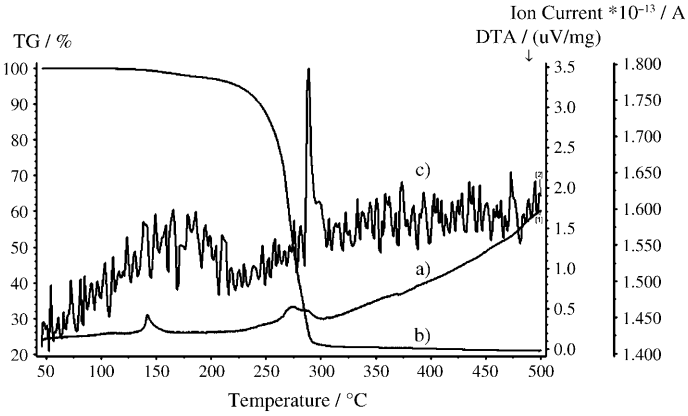

Figure 2. a) DTA, b) TG, and c) QMS curves of the thoroughly washed $[Cu(SC_{12}H_{25})_2]$ precursor, heated from 40 to 500 °C under a N_2 atmosphere. The DTA scale refers to exponential values.

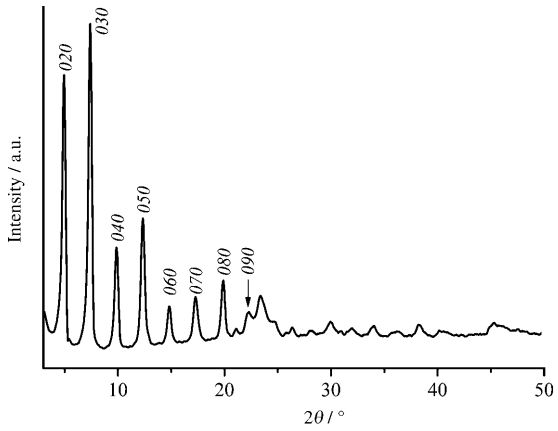

Figure 1. The PXRD pattern ($Cu_{K\alpha}$ radiation) of the $[Cu(SC_{12}H_{25})_2]$ precursor.

curve displays a sharp peak at 142.3 °C that results from cleavage of the C–S bond to generate Cu_2S and a broad peak at 275.9 °C that corresponds to the evaporation of 1-dodecanethiol (of which the boiling point is 266–283 °C). On the other hand, the TG curve shows no weight change up to 143 °C and slight weight loss between 143 and 225 °C, which corresponds to the volatilization of the in situ-generated organic molecule ($C_{12}H_{25}SH$), and rapid weight loss between 225 and 290 °C caused by the evaporation of $C_{12}H_{25}SH$. Therefore, the DTA and TG data suggest the decomposition of the precursor starting at 143 °C, and the remaining of the in situ generated $C_{12}H_{25}SH$ molecule in the reaction system up to 225 °C. The organic molecule, $C_{12}H_{25}SH$, contributes greatly to the control of the morphologies of the uniform Cu_2S nanoproducts (see the LPLP Conversion Mechanism section).

Structure and morphology of the Cu_2S nanoproducts: A representative PXRD pattern of Cu_2S nanoproducts in Figure 3 shows that all the diffraction peaks match well with orthorhombic Cu_2S (JCPDS file no. 02-1294, stored in the International Centre for Diffraction Data). It is the first time that nano Cu_2S has been formed in the orthorhombic phase. Bulk orthorhombic Cu_2S is metastable at low temperature and transforms into hexagonal chalcocite at 103.5 °C.[28] Interestingly, we found that nano orthorhombic Cu_2S continuously transforms into the monoclinic phase, as indicated in Figure 4. For example, nanoparticles produced at 220 °C for 1 h are orthorhombic Cu_2S (JCPDS file no. 02-1294), and those produced after 10 h are monoclinic Cu_2S (JCPDS file no. 83-1462). For extremely long reaction times (7 d) the products are mainly monoclinic Cu_2S (JCPDS file no. 83-1462) with a minor tetragonal phase (JCPDS file no. 72-1071; Figure 5). More interestingly, the *d* values, which correspond to the two most intense diffraction peaks at around 46 and 48° in Figure 4, increase linearly as the annealing time lengthens (see the Supporting Information, Figure S1). These relationships indicate a gradual phase transition that may be caused by the twinning relationship of orthorhombic and monoclinic Cu_2S, as found in previous reports.[29,30]

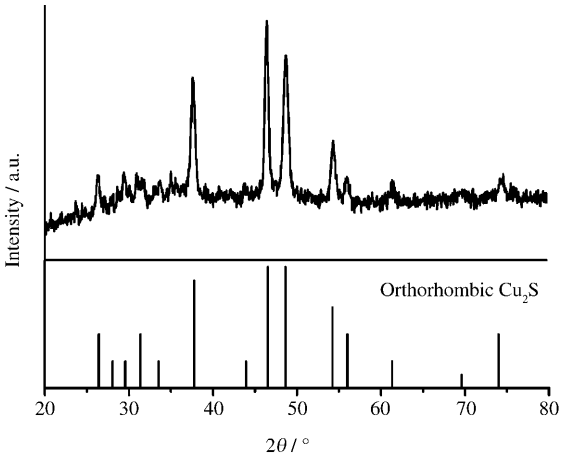

Figure 3. The PXRD pattern of Cu_2S nanoproducts synthesized under N_2 at 210 °C for 10 h. The pattern matches well with orthorhombic Cu_2S (JCPDS file no. 02-1294).

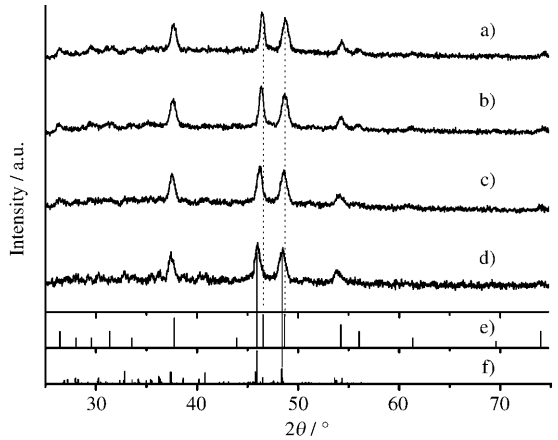

Figure 4. The PXRD patterns of Cu_2S nanoproducts synthesized under N_2 at 220 °C for a) 1, b) 2, c) 4, and d) 10 h. The PXRD patterns for e) orthorhombic and f) monoclinic Cu_2S are also shown.

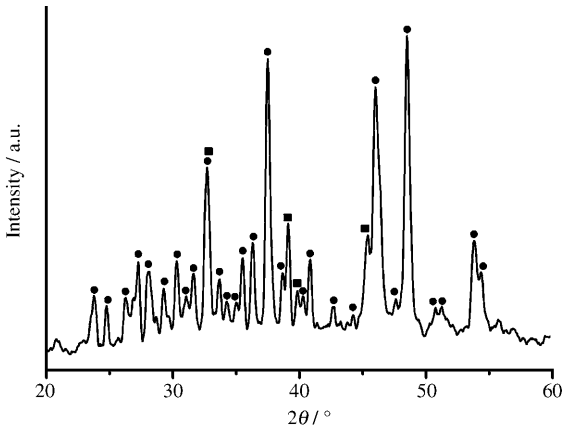

Figure 5. The PXRD pattern of Cu_2S products synthsized under N_2 at 220 °C for 7 days. Peaks marked with ● and ■ match well with monoclinic Cu_2S (JCPDS file no. 83-1462) and tetragonal Cu_2S (JCPDS file no. 72-1071), respectively.

The effects of reaction temperature and time on the morphology have been investigated by performing a batch of experiments loaded with similar amounts of $[Cu(SC_{12}H_{25})_2]$ precursor. The details of each reaction and the descriptions of the products are summarized in Table 1.

Table 1. Experimental conditions for the preparation of Cu_2S nanoparticles of different sizes from $[Cu(SC_{12}H_{25})_2]$ at different annealing temperatures (*T*) and times (*t*).

			Description of the nanoproducts[b]	
T[a] [°C]	t [h]	Morphology[c]	Diameter [nm] (σ [%])	Thickness [nm] (σ [%])
200	2	I	≈3.0	–
200	10	II	25.2 (±16.7)	11.8 (±7.3)
210	2	II	8.3 (±11.8)	–
210	10	III	25.8 (±15.3)	12.0 (±7.1)
220	0.5	I	5.5 (±7.7)	–
220	1	II	21.7 (±24.0)	11.9 (±6.3)
220	2	II	23.2 (±18.5)	12.0 (±5.3)
220	4	II	26.0 (±14.9)	12.3 (±6.5)
220	10	III	27.5 (±14.7)	12.7 (±5.4)

[a] Heating from RT to the desired temperature occurred within 2 h. [b] The morphologies and sizes of nanoproducts were judged from TEM images, and their average diameter and thickness were obtained from count plots (see the Supporting Information, Figures S7–S20). [c] I, II, and III indicate small nanoparticles, nanodisks, and faceted nanodisks, respectively.

Table 1, and these results clearly show that both the reaction temperature and the time influence the size and shape of the Cu_2S nanoproducts. For example, samples annealed for a fixed 2 h showed an increase in diameter from ≈3 to 23.2 nm as the temperature was increased from 200 to 220 °C, and the morphology changed from small particles to disks. Note that the nanodisks shown in Figure 6b also exhibit a typical quasi-close packing.[10] These nanodisks are lying flat on the substrate, which indicates a large diameter-to-thickness ratio. However, the faceted nanodisks in Figure 6c tend to stack together into an extended chain, as indicated by the circled area. Interestingly, some disk-like islands made of these small nanoparticles are produced under N_2 at 200 °C after 2 h (Figure 7). Such small-particle aggregation clearly shows an intermediate from small nanoparticles to nanodisks during the growth process.

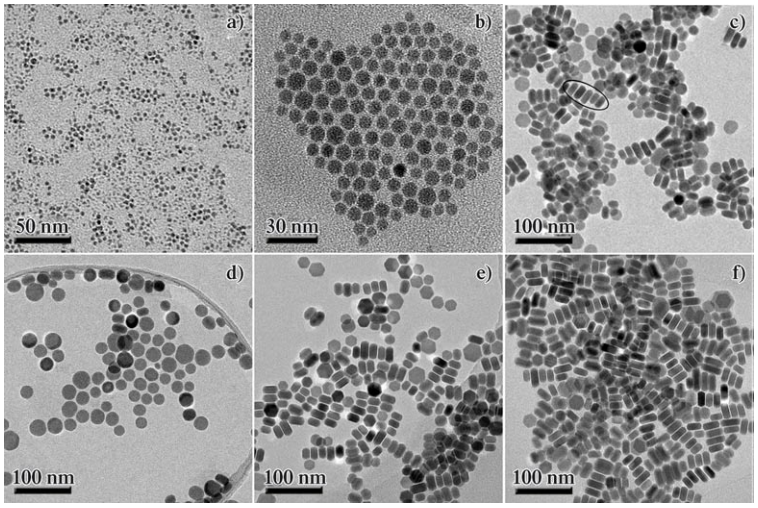

Figure 6. TEM images of Cu_2S nanoproducts produced under N_2 for 2 h at a) 200, b) 210, and c) 220 °C, and for 10 h at d) 200, e) 210, and f) 220 °C.

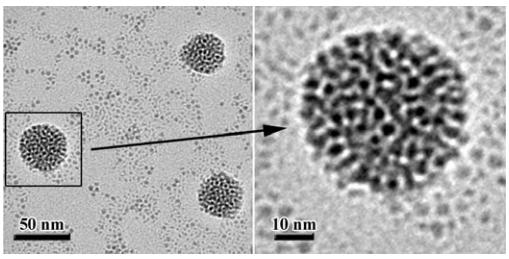

Figure 7. TEM images of small Cu_2S nanoparticles and the fused small-particle aggregation produced under N_2 at 200 °C for 2 h. Right: An enlarged view of the selected area.

Results of parallel experiments annealed for 10 h at these three temperatures are shown in Figure 6d–f, and also reveal the shape evolution from nanodisks (produced at 200 °C) into faceted nanodisks (220 °C). The nanodisks formed at 200 °C are almost all lying flat on the substrate and have a considerable size distribution (Figure 6d); the average diameter is 25.2 nm ($\sigma = \pm 16.7\,\%$). At 210 °C (Figure 6e), some nanodisks tend to stack together into extended chains, a feature that was not seen when the duration time was only 2 h (Figure 6b), and the average diameter increases to 25.8 nm ($\sigma = \pm 15.3\,\%$). Faceted nanodisks were obtained at 220 °C (Figure 6f), most of which are perpendicular to the substrate and stacked together into chain motifs with different lengths and orientations. This stacking motif may reduce the exposed surface areas and, therefore, reduce the surface energy of the nanodisks. In addition, the average diameter of the faceted nanodisks increased to 27.5 nm ($\sigma = \pm 14.7\,\%$).

The TEM images of the products of four parallel reactions annealed at 220 °C for 30 min, 1, 4, and 10 h are shown in Figure 8. The monodispersed nanoparticles are produced by annealing for 30 min and have an average diameter of 5.5 nm ($\sigma = \pm 7.7\,\%$, Figure 8a), and have a quasi-close-packed assembly similar to that in Figure 6b. The other three reactions produce nanodisks, and as the reaction time was increased from 1 (Figure 8b) to 4 h (Figure 8c), the number of perpendicular faceted nanodisks is increased. After annealing for 10 h (Figure 8d), nearly all of the nanodisks are faceted. Judging from the PXRD patterns and TEM images, the monoclinic phase tends to show faceted disk morphology, this is in agreement with the generally accepted fact that

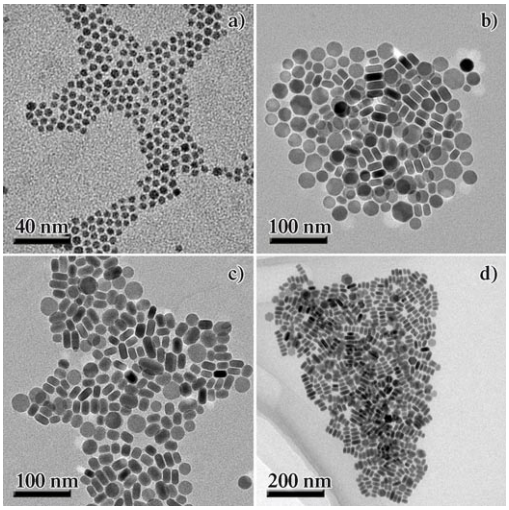

Figure 8. The TEM images of Cu_2S nanoproducts produced under N_2 at 220 C for a) 30 min, b) 1, c) 4, and d) 10 h.

longer annealing times give better crystallinity. The metastable orthorhombic Cu_2S shows worse crystallinity and gives less clear HRTEM images that provide no detailed structural information.

When the faceted nanodisk stands perpendicularly to the substrate, it looks like a rod, thus the thickness of the disks is defined as the width of the rod and was also measured. This disk–rod relationship has also been confirmed by the tilted TEM observations (see the Supporting Information, Figure S2). Interestingly, all our experiments (Table 1) indicate that these nanodisks show a visible increase in diameter with increasing temperature or prolonged annealing time, but a negligible change in thickness. For example, as the annealing time is extended from 1 to 10 h, an obvious increase in diameter ($\approx$27%) was found, whereas only a 7% increase in thickness was found (Table 1). This indicates that the growth of the lamellar nanoproducts is substantially anisotropic. A more detailed discussion of growth mechanism is presented below.

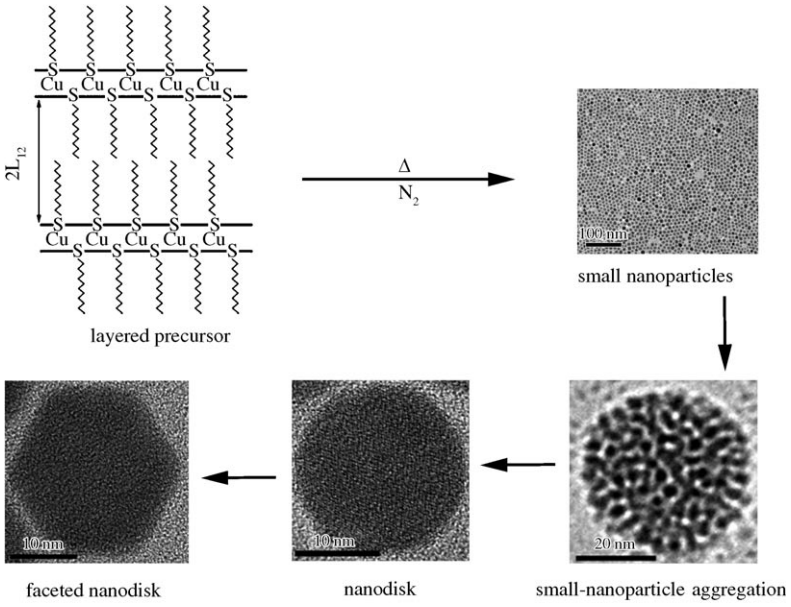

Figure 9. The supposed mechanism of conversion from the layered precursor (top left) to small nanoparticles (top right) to small-particle aggregation (bottom right) to nanodisks (bottom middle) to faceted nanodisks (bottom left).

The LPLP conversion mechanism: In the previous report on Ag nanodisks,[18] we mentioned that the formation of nanodisks involves two processes, nucleation and growth, which are controlled by the crystal structure of the precursor. However, direct TEM observation is lacking because of the difficulty of separating small Ag nanoparticles from the AgSR precursor shortly after firing. The subsequent research on Bi has provided a substantial intermediate, Bi-nanofilm that is several atoms thick, to prove that the nucleation and early growth of the nanoparticles are indeed constrained by the crystal structure of the precursor. The low reaction temperature of the Bi system allows the capture of the nanofilm intermediate, which is impossible in the Ag system. On the other hand, the low melting point of Bi makes the fusion and conglomeration of small particles remarkably speedy, so an intermediate for such interparticle growth is undetectable. Herein, small Cu_2S nanoparticles have been repeatedly obtained because interparticle growth occurs well after the complete decomposition of the precursor. We were thus able to capture an intermediate of this interparticle growth; this is significant because intermediates are usually metastable, and can rarely be observed in different and suitable systems. Bi-nanofilm[19] and these intermediates in different systems, for example, Bi, Ag, Cu_2S, have been integrated to investigate the nucleation and growth process of the structure-controlling solventless synthesis.

The LPLP conversion mechanism of Cu_2S is sketched in Figure 9. First, small Cu_2S nanoparticles are produced under low temperature or short reaction times, such as 200°C for 2 h or 220°C for 30 min. These small Cu_2S nanoparticles tend to arrange in a quasi-layered pattern that is thought to be restrained by the layered structure of the $[Cu(SC_{12}H_{25})_2]$ precursor. The in situ-generated $C_{12}H_{25}SH$ can distribute on both sides of this assembly by absorbance on the surface of each Cu_2S particle. During the subsequent heat treatment, these small nanoparticles fuse into disk-like islands (Figure 7) by an aggregation and coalescence process. The quasi-layered distribution of small nanoparticles leads to isotropic intralayer and anisotropic interlayer diffusions. The hindrance of the long organic chains also results in a "long path" for interlayer diffusion. During the subsequent crystallization of the islands into nanodisks, the growth in diameter is thus markedly faster (intralayer diffusion) than that of thickness (interlayer diffusion). As shown in Figures 6 and 8, the thickness shows no significant increase, as described above. Eventually, faceted nanodisks with hexagonal symmetry are crystallized (see the Supporting Information Figure S3).

Note that $C_{12}H_{25}SH$ has a crucial impact on the disk morphology. A parallel experiment was designed as follows: Faceted nanodisks formed at 220°C for 2 h (Table 1) were thoroughly washed with dichloromethane until free of $C_{12}H_{25}SH$. The absence of $C_{12}H_{25}SH$ was verified by checking for the characteristic vibrations in the FTIR spectrum (see the Supporting Information, Figure S4). Once free of

$C_{12}H_{25}SH$, the pure Cu_2S nanodisks were re-annealed at 220 °C for 2 h. The results show agglomerative Cu_2S chunks that are totally different from the nanodisks formed in the presence of $C_{12}H_{25}SH$ (see Figure S5 in the Supporting Information and Figure 8c).

Optical properties: The UV/Vis absorption spectra of suspensions of Cu_2S nanoproducts in CH_2Cl_2 are shown in Figure 10. Small Cu_2S nanoparticles with diameters less than

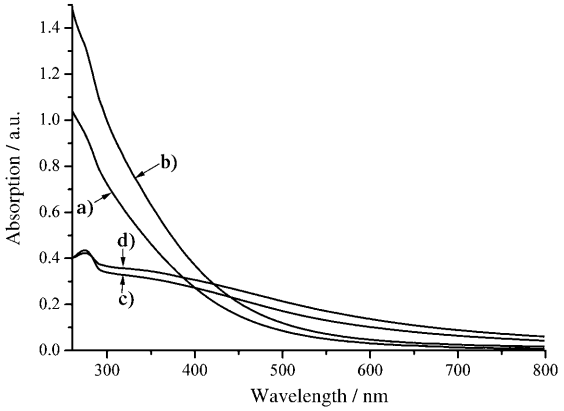

Figure 10. RT UV/Vis absorption spectra of suspensions of a) small Cu_2S nanoparticles (diameter ≈3 nm), b) small Cu_2S nanoparticles (diameter 5.5 nm), c) Cu_2S nanodisks (diameter 21.7 nm, thickness 11.9 nm), and d) Cu_2S nanodisks (diameter 26.0 nm, thickness 12.3 nm) in dichloromethane.

6 nm (average diameter ≈3 or 5.5 nm) display similar spectra (curves a and b) that both lack a sharp maximum. The general explanation is that the sizes of the nanoparticles are smaller than the exciton bohr radius. Unfortunately, the exciton bohr radius of Cu_2S is not available. However, it is likely to be larger than 5.5 nm, because both 3 nm and 5.5 nm particle samples exhibit absorption edges at around 475 nm, which show clear blueshifts compared with that of bulk Cu_2S (1022 nm).[23] The absence of sharp maxima in these two absorption spectra indicates that the dispersed size distribution is in agreement with the TEM observations (Figure 6a, Figure 7a).

Two nanodisk samples with diameters of 21.7 and 26.0 nm, respectively, exhibit a sharp absorption peak at 274 nm. The overall absorption behavior is similar to that of Cu_2S nanowires.[24] Distinctively, different diameters change the position of the absorption peak of Cu_2S nanowires,[24] but not in the case of our nanodisks. It is possible that the smaller dimension (thickness vs. diameter) governs the band-gap energy, as found in ZnS sheets.[31] The TEM observations suggest a nearly constant thickness for the as-synthesized nanodisks, therefore two nanodisk samples with different diameters have the same absorption maximum. The average thickness of the nanodisks can be calculated according to the band-gap-energy shift (ΔE_g) in Equation (1):[32]

$$\Delta E_g \approx \frac{h^2}{8\mu_y L_y{}^2} \quad (1)$$

in which μ_y is the reduced effective mass of the exciton and L_y is the crystallite thickness. Therefore, $\Delta E_g \times L_y{}^2$ should be a constant. The value of $\Delta E_g \times L_y{}^2$ calculated from Cu_2S nanoribbons[26] is 40.96 eV nm^2. As shown in Figure 10, the absorption maximum at $\lambda = 274$ nm and the absorption edge at $\lambda = 293$ nm (curves c and d), give $\Delta E_g = 0.29$ eV, and the average thickness is then calculated to be ≈12 nm, which is in good agreement with the thickness obtained from TEM observations.

The optical diffuse reflectance spectra of Cu_2S nanodisks have also been measured and are plotted in Figure 11. Tauc's plots by the extrapolation method give E_g values of 2.03 and 1.99 eV for 21.7 and 26.0 nm nanodisks, respectively. Both samples exhibit blue band-gap shifts compared with bulk Cu_2S, which indicates a strong quantum size effect.

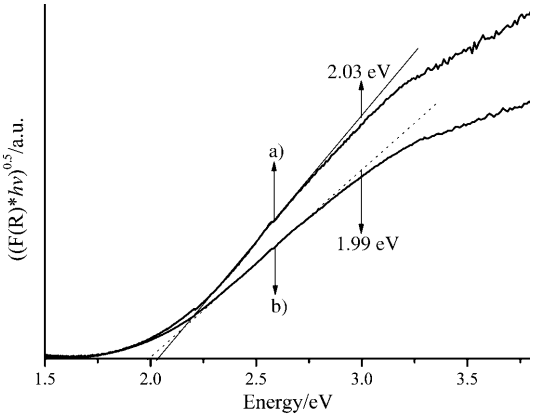

Figure 11. Tauc's plots for the estimation of the band gaps of Cu_2S nanodisks with a) diameter 21.7 nm, thickness 11.9 nm and b) diameter 26.0 nm, thickness 12.3 nm.

Conclusion

In summary, uniform Cu_2S nanoproducts have been obtained from a layered copper-thiolate precursor. The nearly constant thickness of the faceted nanodisks with different diameters suggests isotropic growth. This isotropic growth is thought to be restrained by the physical arrangement of the small particles (Figures 6b and 7a), which was highly influenced by the layered crystal structure of the precursor during the nucleation stage. The anisotropic interparticle growth is also influenced by the in situ-generated RSH molecules. Interestingly, the ripening and crystallization of these nanodisks reveal a continuous orthorhomic-to-monoclinic phase transition process. These nanoproducts show an increase in the band gap and a blueshift of the absorption edge compared with that of bulk Cu_2S.

Finally, the Cu_2S small-particle aggregation intermediate substantiates that both the nucleation process and the late growth process (i.e., the interparticle growth stage) in this

structure-controlling solventless method are controlled by the layered crystal structure of the precursor and the thiol byproduct.

Experimental Section

Chemicals: 1-Dodecanethiol ($C_{12}H_{25}SH$, 98%, Labcaster), copper nitrate ($Cu(NO_3)_2{\cdot}3H_2O$, A.R., Shanghai), ethanol (A.R., Shanghai), and dichloromethane (A.R., Shanghai) were used as purchased without further purification. N_2 gas (99.99%) was purchased from Fuzhou Xinhang Gas Co.

Synthesis of the $[Cu(SC_{12}H_{25})_2]$ precursor: 1-Dodecanethiol (19.3 mL, 80 mmol) was dissolved in ethanol (40 mL), then aqueous copper nitrate (20 mL, 1.0 mol L^{-1}) was slowly added to the mixture with vigorous stirring to give a yellow-green suspension. After stirring for 30 min, the precipitation was collected by filtration, washed two or three times with distilled water and ethanol to ensure the removal of all soluble materials, and then dried in an evacuated vacuum desiccator to remove the residual solvent. Finally, the yellow-green powdery precursor (9.250 g) was obtained (99.2% yield based on Cu, indicating complete precipitation of the Cu^{2+} ions). Elemental analysis calcd (%) for $[Cu(SC_{12}H_{25})_2]$: C 61.8, H 10.8, N 0, S 13.8; found: C 62.3, H 10.7, N $<$0.3, S 13.7.

Syntheses of Cu_2S nanodisks: In a representative reaction, $[Cu(SC_{12}H_{25})_2]$ (0.694 g) was placed in a small Pyrex tube (1.5×15 cm) and transferred into a larger long jacket Pyrex tube (6 cm×1 m), which was capped on both ends by stoppers with gas outlets, purged with N_2 gas for 5 min, heated in a program-controlled tube furnace at 220°C for 10 h, and allowed to cool to RT by radiation in the furnace. The yellow-green precursor turned black after heating (see the Supporting Information, Figure S6). The raw product was dispersed in dichloromethane, centrifuged at 4000 rpm for 5 min to remove the byproducts, and then collected (0.108 g, 91.3% yield based on the amount of $[Cu(SC_{12}H_{25})_2]$). The experimental conditions for Cu_2S nanoproducts are summarized in Table 1. The black product was characterized to be nano Cu_2S (see the Results and Discussion Section). The Cu:S stoichiometry was further confirmed to be 1.99:1.00 by elemental analysis.

Sample characterization: Powder X-ray diffraction (PXRD), scanning electron microscopy (SEM), transmission electron microscopy (TEM), and high-resolution TEM (HRTEM) were used to characterize the crystal structure, composition, size, and shape of the products, respectively. The SEM images were obtained by using a JSM 6700F scanning electron microscope equipped with a field emission gun operating at 10 kV. The TEM and HRTEM images were obtained by using a JEM 2010 transmission electron microscope equipped with a field emission gun operating at 200 kV. The digital images were obtained by using the imaging software system (DigitalMicrograph 3.11.2) designed for a Gatan multipole scanning CCD camera. For TEM observation, each sample was prepared by depositing a drop of a dilute suspension of the corresponding nanoproduct in dichloromethane onto a 200 mesh carbon-film-coated Cu grid. Elemental analyses were performed by using a Vario EL III instrument (Elementar Co.) for C, H, N, and S and an Ultima-2 inductively coupled plasma optical emission spectrometer (ICP-OES) for Cu. The PXRD patterns were collected at room temperature with the aid of a Rigaku DMAX 2500 powder diffractometer with ultra 18 kW $Cu_{K\alpha}$ radiation. The DTA/TG/QMS measurements were performed by using a NETZSCH STA449C instrument in connection with a QMS403C spectrometer. The UV/Vis absorption and diffuse-reflectance spectra were measured by using a Perkin–Elmer Lambda-900 spectrophotometer. The optical band gaps of the Cu_2S nanodisks were estimated by using a Tauc's plot.[32]

Acknowledgements

This research was supported by the National Natural Science Foundation of China (projects 20773130, 20521101, 2073303, and 20803080), the State Key Laboratory Science Foundation (070023 and 050097), the Fujian Institute of Research on the Structure of Matter (FJIRSM) (Key Project, SZD07004), the Chinese Academy of Sciences (CAS) (Key Project, KJCX2-YW-H01), and the Knowledge Innovation Program of the CAS.

[1] M. Bruchez, Jr., M. Moronne, P. Gin, S. Weiss, A. P. Alivisatos, *Science* **1998**, *281*, 2013–2016.
[2] J. Planelles, J. G. Díaz, J. Climente, W. Jaskolski, *Phys. Rev. B* **2002**, *65*, 245302.
[3] U. J. Woggon, *Appl. Phys.* **2007**, *101*, 081727.
[4] M. A. El-Sayed, *Acc. Chem. Res.* **2004**, *37*, 326–333.
[5] W. E. Buhro, V. L. Colvin, *Nat. Mater.* **2003**, *2*, 138–139.
[6] F. Dumestre, B. Chaudret, C. Amiens, P. Renaud, P. Fejes, *Science* **2004**, *303*, 821–823.
[7] M. S. Gudiksen, L. J. Lauhon, J. Wang, D. C. Smith, C. M. Lieber, *Nature* **2002**, *415*, 617–620.
[8] X. F. Duan, Y. Huang, Y. Cui, J. F. Wang, C. M. Lieber, *Nature* **2001**, *409*, 66–69.
[9] H. Zeng, P. M. Rice, S. X. Wang, S. H. Sun, *J. Am. Chem. Soc.* **2004**, *126*, 11458–11459.
[10] H. T. Zhang, G. Wu, X. H. Chen, *Langmuir* **2005**, *21*, 4281–4282.
[11] Y. C. Cao, *J. Am. Chem. Soc.* **2004**, *126*, 7456–7457.
[12] S. H. Chen, D. L. Carroll, *Nano Lett.* **2002**, *2*, 1003–1007.
[13] X. S. Du, Z. Z. Yu, A. Dasari, J. Ma, Y. Z. Meng, Y. W. Mai, *Chem. Mater.* **2006**, *18*, 5156–5158.
[14] M. B. Sigman, A. Ghezelbash, T. Hanrath, A. E. Saunders, F. Lee, B. A. Korgel, *J. Am. Chem. Soc.* **2003**, *125*, 16050–16057.
[15] A. Ghezelbash, M. B. Sigman, B. A. Korgel, *Nano Lett.* **2004**, *4*, 537–542.
[16] M. B. Sigman, B. A. Korgel, *Chem. Mater.* **2005**, *17*, 1655–1660.
[17] L. Chen, Y. B. Chen, L. M. Wu, *J. Am. Chem. Soc.* **2004**, *126*, 16334–16335.
[18] Y. B. Chen, L. Chen, L. M. Wu, *Inorg. Chem.* **2005**, *44*, 9817–9822.
[19] J. Chen, L. M. Wu, L. Chen, *Inorg. Chem.* **2007**, *46*, 586–591.
[20] J. Chen, L. Chen, L. M. Wu, *Inorg. Chem.* **2007**, *46*, 8038–8043.
[21] F. Pfisterer, *Thin Solid Films* **2003**, *431*, 470–476.
[22] G. M. Liu, T. Schulmeyer, J. Brotz, A. Klein, W. Jaegermann, *Thin Solid Films* **2003**, *431*, 477–482.
[23] S. K. Haram, A. R. Mahadeshwar, S. G. Dixit, *J. Phys. Chem.* **1996**, *100*, 5868–5873.
[24] Z. P. Liu, D. Xu, J. B. Liang, J. M. Shen, S. Y. Zhang, Y. T. Qian, *J. Phys. Chem. B* **2005**, *109*, 10699–10704.
[25] Q. Y. Lu, F. Gao, D. Y. Zhao, *Nano Lett.* **2002**, *2*, 725–728.
[26] C. N. Chen, C. L. Zhu, L. Y. Hao, Y. Hu, Z. Y. Chen, *Chem. Lett.* **2004**, *33*, 898–899.
[27] Z. Q. Li, H. Yang, Y. Ding, Y. J. Xiong, Y. Xie, *Dalton Trans.* **2006**, 149–151.
[28] S. Pakeva, K. Germanova, *J. Phys. D* **1985**, *18*, 1371–1376.
[29] F. Gronvold, E. F. Westrum, *J. Chem. Thermodyn.* **1987**, *19*, 1183–1198.
[30] T. D. Sands, J. Washburn, R. Gronsky, *Phys. Status Solidi* **1982**, *72*, 551–559.
[31] S. H. Yu, M. Yoshimura, *Adv. Mater.* **2002**, *14*, 296–300.
[32] J. Tauc, R. Grogorovici, A. Vancu, *Phys. Status Solidi* **1966**, *15*, 627.

Received: July 18, 2008
Published online: November 10, 2008

